Creating Viable FEA Material Representations for Elastomers Using Non-Ideal Test Data

Ted Diehl[1,2], Yu Xu[1]

[1]DuPont Engineering Technology, Chestnut Run, Bldg 722, Wilmington, DE 19880-0722
Ted.Diehl@USA.DuPont.com, Yu.Xu@USA.DuPont.com

[2]Bodie Technology, Inc., PO Box 1024, Unionville, PA 19375-1024
Ted.Diehl@BodieTech.com

Abstract: *Most automated material fitting procedures in commercial FEA codes assume that "ideal tests" are used to generate measured material data. Unfortunately, there are many scenarios where only "non-ideal" test data are available. This paper presents two case studies that highlight various strategies to transform and/or salvage such distorted test data so that viable FEA material representations can be created. Two examples are presented: (1) The hyperelastic characterization of a nearly incompressible elastomer that is manufactured with a stiff PET film on one side which prohibits the use of planar shear testing and distorts data from puck compression testing and (2) The characterization of nearly incompressible elastomers reinforced by short stiff fibers.*

Keywords: *Hyperelastic, hyperelasticity, rubber, orthotropic, material fitting, material parameter determination, material law tuning, salvaging data, averaging multiple data curves, nonlinear FEA, nonlinear Finite Element Analysis, Abaqus, Mathcad, Kornucopia.*

1. Introduction

The accuracy of finite element analyses is highly dependent on the accuracy of the material models used in such simulations. This is especially true with elastomeric (rubber) materials as their constitutive characterization can be a rather daunting task. A partial list of items to consider when creating a material model for a nearly incompressible elastomer includes:

- What are the deformation modes of interest (uniaxial, biaxial, shear, volumetric, and/or something else)? Are the strains anticipated to be small (< 10 %) or large (25%, 50%, 100%, or more)? Will these deformations be predominantly tension or compression?
- Is the model intended for a virgin sample or one that has been previously deformed (and by how much, how often, at what rate, and in what modes)? Will the model be elastic, or does inelasticity need to be included also? Is loading intended to be quasi-static or at rate, will it be monotonic or will unloading also need to be simulated?

- Is the material isotropic or anisotropic? Even if it is anisotropic, can we "get away" with an isotropic approximation?

Answers to these kinds of questions will impact the type of experiments required to create a viable material model. And once the measured test data are obtained, all that remains is to curve-fit the data to one or more possible material laws (Neo-Hooke, Arruda-Boyce, Ogden-Hill, Polynomial, etc). This last part has a big assumption of course — namely that the test data are "ideal" and reasonably satisfy the geometry and boundary conditions assumed for the primitive deformation modes that the material model calibration process is likely to utilize.

In many cases experimental measurements are not ideal because they are influenced by boundary conditions and other issues such as some amount of material anisotropy. With nearly incompressible elastomers, significant data distortions can occur because of the interaction of a high bulk modulus, sample geometry aspect ratios, and fixture clamping. The amount and type of distortion is highly dependent on deformation mode. Compression tests on blocks or pucks are often problematic because the ideal uniaxial compressive state assumed by the calibration software (or equations) is not satisfied by the actual test. The experiment will have some amount of non-uniform transverse deformation caused by the interaction of the sample and the loading platens which, due to the high bulk modulus, can distort the measured apparent loads and stresses by large amounts compared to what an ideal uniaxial test would produce (factors of 2 to over 50 are not uncommon). This is even true when the loading platen is lubricated (more will be said about this in Section 3).

This paper discusses methodologies that allow the user to combine theoretical analysis, measured data, and FEA to adjust ("correct") measured data so that improved material model calibrations can be obtained. To achieve this, we will look closely at the physics of the tests and materials and then make physically-motivated adjustments to data as needed to find the best material coefficients. In many cases these adjustments will be based on a combination of transformations from theoretical equations combined with scaling factors derived from FEA studies. To ensure that the resulting material models and coefficients are valid, we always compare our final material models back to the original un-modified test data by running FEA models that attempt to include all the non-ideal behavior that existed in the original experimental set-ups. The two case studies presented highlight various strategies to transform and/or salvage such distorted test data.

2. Characterizing a nearly incompressible elastomeric sheet that is constrained by a stiff PET film on one side

Figure 1 depicts an elastomeric sheet that is manufactured with a PET film bonded on one side. The goal of the analysis is to characterize the sheet so that FEA simulations of "general-purpose deformations" can be created. These models are expected to contain large amounts of compression (y-direction) and shear (in all three directions). By physical inspection and past experience, it is evident that the PET properties are significantly stiffer (~1000 time) than the elastomer. Figure 1 lists the relevant properties of the PET skin.

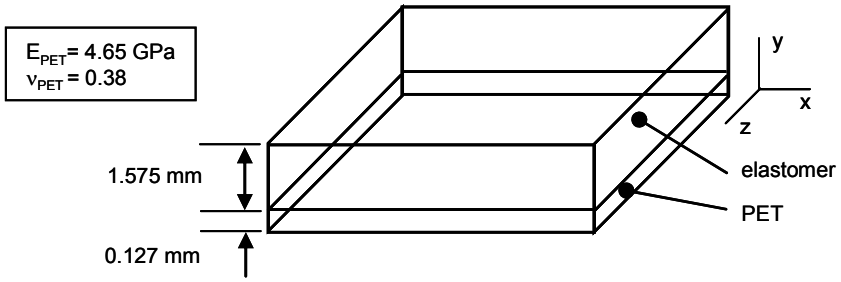

Figure 1: Depiction of elastomeric sheet with PET film adhered to bottom.

Because the PET is bonded to the elastomer, it is very difficult to isolate the elastomer for material testing. Hence, it will be challenging to obtain a good hyperelastic characterization of the elastomeric component from physical testing of the entire sheet. Any type of testing in-plane (xz plane) will be almost useless as the PET behavior will dominate. Since the sheet is available in only one thickness, namely 1.575 mm, testing modes will be limited. For initial material evaluation, the tests selected are uniaxial compression (in the y-direction) and simple shear (in the xy or yz directions). It is emphasized that the classic planar test (so-called pure shear) is impractical for this specimen geometry given the fact that it is very difficult to separate the PET from the elastomer.

Figure 2a presents *apparent* nominal stress vs. *apparent* nominal strain data for uniaxial puck compression experiments of three different specimen diameters. All data was on samples that were pre-cycled to "break-in" the elastomer. In addition to the nearly rigid radial constraint from the PET on the bottom of the specimen, the high coefficient of friction between the platen and elastomer sample at the top produced yet an additional radial constraint (no slip). The data is *apparent* because the actual strain and stress state in each specimen is non-uniform and unknown due to boundary condition effects and non-uniform bulging (see Figure 3c). The apparent stress is computed by simply dividing the applied compressive force by the original cross-sectional area of the sample, *d*, and the apparent compressive strain is the platen displacement divided by the initial thickness, *t*, of the elastomer (Figure 2a). It is again noted that the PET deformation is essentially rigid due to its stiff modulus compared to the elastomer. Using general purpose averaging and other data manipulation functionality from Kornucopia®, (www.BodieTech.com) the data curves were readily averaged and initial moduli were computed. This data clearly demonstrates the level of distortion that can occur by non-ideal boundary conditions with nearly incompressible materials; the apparent modulus as a function of specimen diameter relative to thickness varied from 14.9 MPa to 86.2 MPa for the range of d/t ratios measured.

Also presented in Figure 2b is the simple shear data. This data looks reasonably linear and because L/H = 23 (a large ratio), the data is believed to be undistorted (Diehl, 1995, Chapter 2.1.1). During the simple shear test, Poynting stress data was also measured, but it is not presented since its value was essentially zero over the entire shear range measured. It is noted that typical Poynting stress response in solid elastomers is very different from foamed elastomers – in foams the Poynting stress will typically be essentially zero below around 5% nominal shear strain, but above 5% the Poynting stress in foams will become positive with significant values.

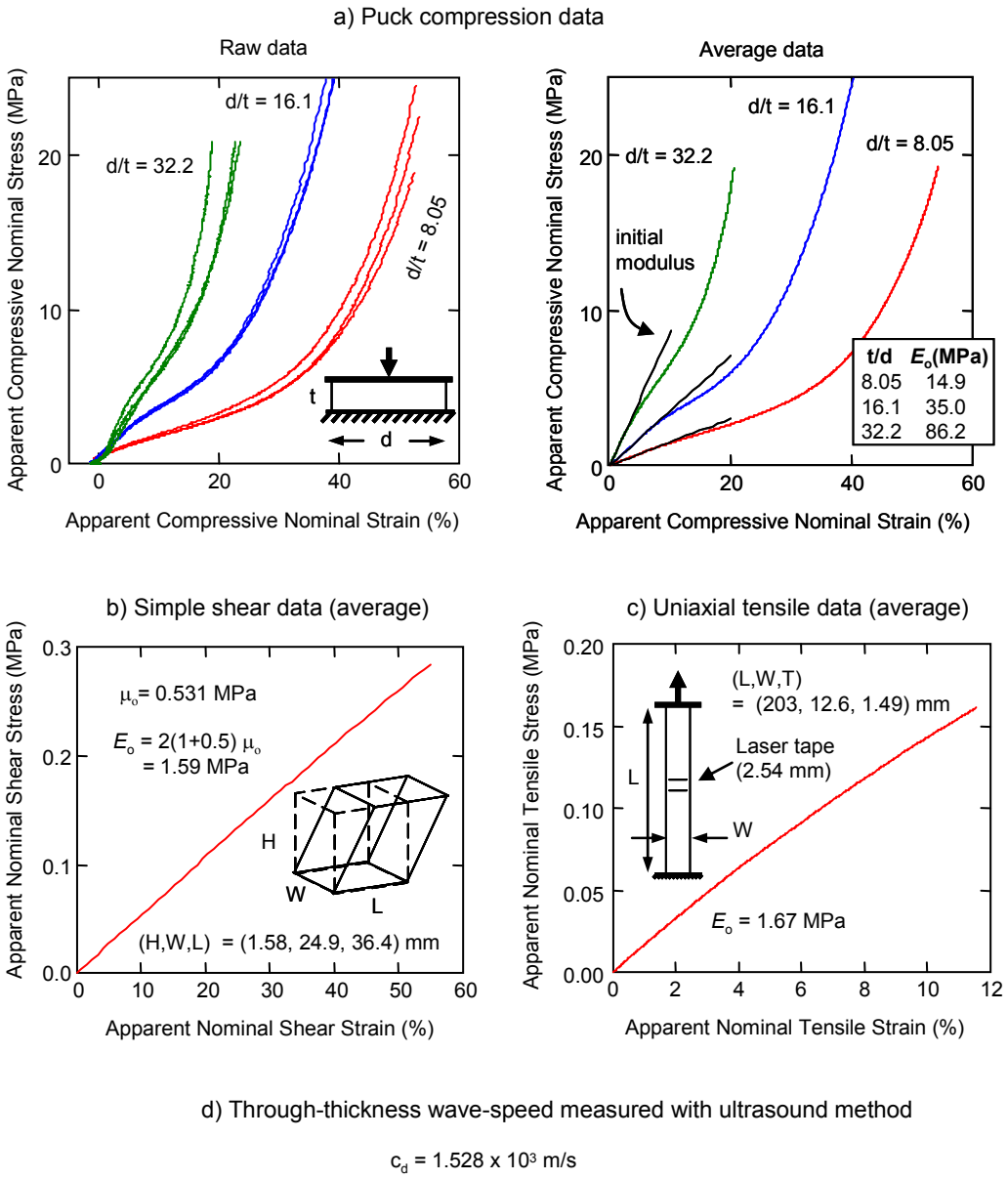

Figure 2: Experimental data derived from samples cut from an elastomeric sheet that was constrained on one side by a 0.127 mm PET sheet. Simple shear and uniaxial tensile data are average curves computed from multiple specimen replicates.

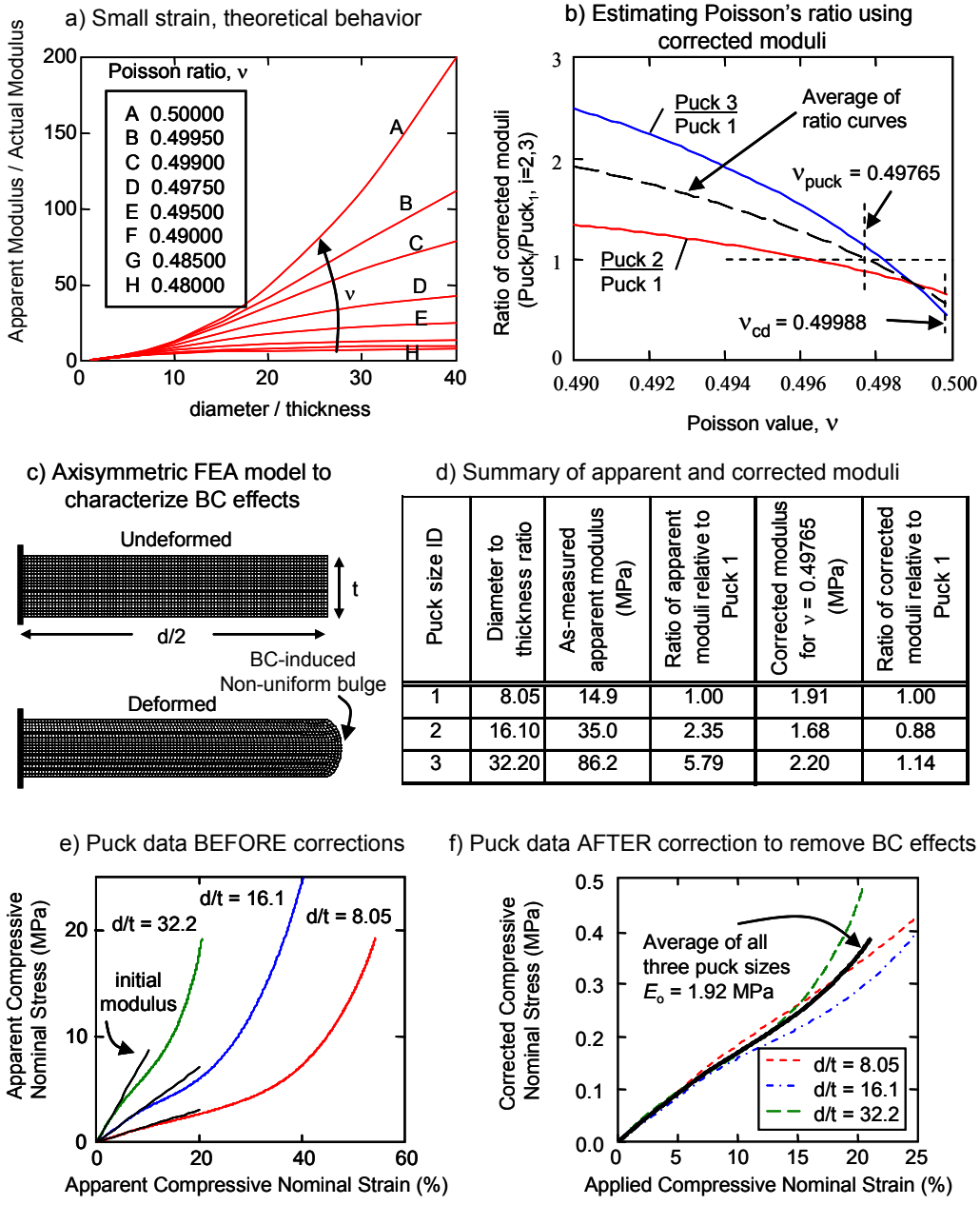

Puck size ID	Diameter to thickness ratio	As-measured apparent modulus (MPa)	Ratio of apparent moduli relative to Puck 1	Corrected modulus for ν = 0.49765 (MPa)	Ratio of corrected moduli relative to Puck 1
1	8.05	14.9	1.00	1.91	1.00
2	16.10	35.0	2.35	1.68	0.88
3	32.20	86.2	5.79	2.20	1.14

Figure 3: Using a small-strain uniaxial compression FE study of the influence of Poisson's ratio and diameter to thickness ratio to "correct" measured test data for improved estimation of modulus, compression stress/strain response, and Poisson ratio estimation.

To further characterize the elastomer, additional tests were performed (Figure 2c-d): Uniaxial tension and a through-thickness wave-speed measurement using an ultrasound method. The uniaxial test specimens were solely elastomeric material that was painstakingly trimmed out of the sheets. Due to small nicks in the trimmed specimens, tensile strains were limited to ~10%. Wave-speed data, which was adjusted to account for the PET contribution, was used to estimate the Poisson's ratio of the elastomer. This was done using formulae from linear isotropic elasticity (Diehl, 1995), namely:

$$\nu = \frac{2\mu - \rho \cdot c_d^{\,2}}{2\mu - 2\rho \cdot c_d^{\,2}} = \frac{E - \rho \cdot c_d^{\,2}\sqrt{E^2 - 10E \cdot \rho \cdot c_d^{\,2} + 9\rho^2 \cdot c_d^{\,4}}}{4\rho \cdot c_d^{\,2}} \qquad \textbf{(1)}$$

Using the above formulae, a value of $\nu_{cd} = 0.49988$ was estimated where the subscript "cd" denotes an estimate based on a wave-speed measurement. It is important to note that the extra digits are included because with nearly incompressible materials, the "first non-nine number" after the 0.49 location is the most significant one.

While the simple shear and uniaxial data of Figure 2 appear to be nearly ideal, the uniaxial compression data in the same figure is clearly distorted. Figure 3 presents a summary of an analysis method that utilizes small-strain FEA results to adjust the distorted compression data, compensating for the unwanted boundary effects. Figure 3a presents data from 64 FEA models that demonstrate how, for a Hookean material, the ratio of the apparent modulus, E_{app}, to the actual modulus, E, increases as a function of the diameter to thickness ratio of the specimen and as a function of the material's actual Poisson's ratio. The FEA models were all small-strain perturbation analyses with radial constraints at the top and bottom surfaces which resulted in non-uniform bulging as depicted in Figure 3c. Using a 2-D interpolation approach, this data can then be used to estimate the actual modulus from apparent compression data as a function of diameter to thickness ratios and Poisson's ratio. If the approach is correct, then after "adjustment factors" are applied to various apparent compression moduli from Figure 2, the Young's moduli should all collapse to a common value. When this was attempted using the wave-speed estimate of Poisson's ratio, the adjusted apparent modulus values were improved, but still had noticeable discrepancies (~50%). Figure 3b generalized the analysis concept by allowing the Poisson's ratio to vary to see if a value could be found that would collapse all the apparent moduli values to a single common value. This analysis indicated that the best result obtained was with a Poisson's ratio of 0.49765 (as compared to the wave-speed estimate of 0.49988). This 0.49765 estimate of Poisson's ratio resulted in the apparent moduli collapsing to within 14% of each other for the three different *d/t* ratios (a huge improvement from the initial apparent moduli ratios of 135% and 479% from Figure 2a). Figure 3e-f shows how this "adjustment methodology" can be further applied to the entire apparent nominal stress/strain curve — the three apparent stress/strain curves collapse very well to a single master curve. This implies that we have reasonably "corrected" the original experimental data to compensate for the non-ideal boundary conditions.

Returning to the simple shear data from Figure 2, it looks clean. However, Abaqus' built-in hyperelastic material calibration (Abaqus, V6.9) for `*Hyperelastic` material models does not support simple shear test data (simple shear test data is only supported for `*Hyperfoam` material

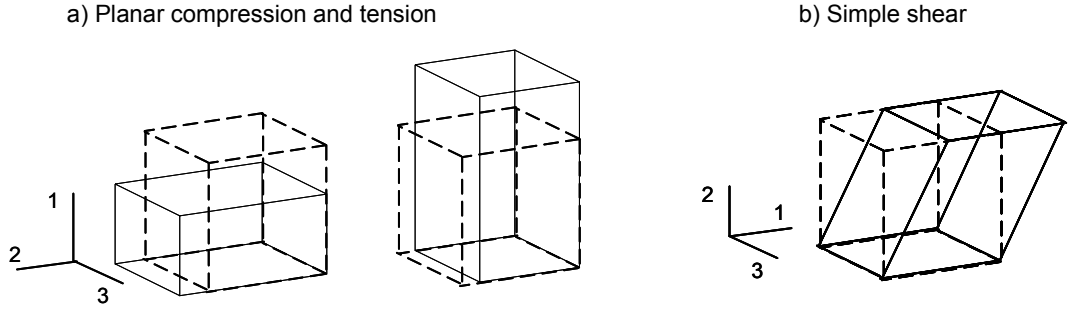

Figure 4: Depiction of ideal planar (so-called pure shear) deformation mode and simple shear deformation mode.

models). Abaqus does support *`Hyperelastic` material calibration using planar data (so-called pure shear). Figure 4 depicts both planar and simple shear deformation modes. From basic equations of mechanics, a direct transformation between shear strain and shear stress (γ, τ) from simple shear and Biot (nominal) strain and nominal stress (ε_b, T) from planar deformation can be derived, namely:

$$\varepsilon_b = \sqrt{1+\frac{1}{2}\gamma^2+\frac{1}{2}\gamma\sqrt{4+\gamma^2}}-1 \qquad \textbf{(2)}$$

$$T = \frac{\tau\sqrt{4+\gamma^2}}{\varepsilon_b+1} \qquad \textbf{(3)}$$

The following points are noted regarding this set of transformation equations. The derivation was for arbitrarily large strain deformations. Poynting stress terms from simple shear were included, but the Poytning stress terms cancelled-out and thus do not appear in the equations above. The fact that a nearly incompressible material has a volume ratio near unity, J≈1, was utilized.

Figure 5a presents the final form of the experimental data supplied to the Abaqus material calibration functionality, namely the planar data based on transforming the simple shear data from Figure 2b using Equations 2 and 3 and a scaled version of the adjusted puck compression curve from Figure 3f (scaled by the ratio of its initial modulus to a value of E derived from the simple shear test data via $E = 2\mu\cdot(1+\nu)$). The basic idea behind this last scaling is that the initial modulus, E, of the two data sets were slightly inconsistent and since the shear data has the least amount of boundary condition distortions, it was assumed to be more accurate. Also presented in Figure 5a are the best-fit Neo-Hooke and Arruda-Boyce models produced by Abaqus calibration. Several other hyperelastic models were investigated, but they either yielded worse fits or had instabilities within the deformation range of interest. It is further noted that since the locking stretch, λ_M, for Arruda-Boyce is 7.0 in this fit, the Arruda-Boyce model will be nearly identical to the Neo-Hooke model for the deformations evaluated in this investigation (initial shear modulus μ_o = 0.461 MPa).

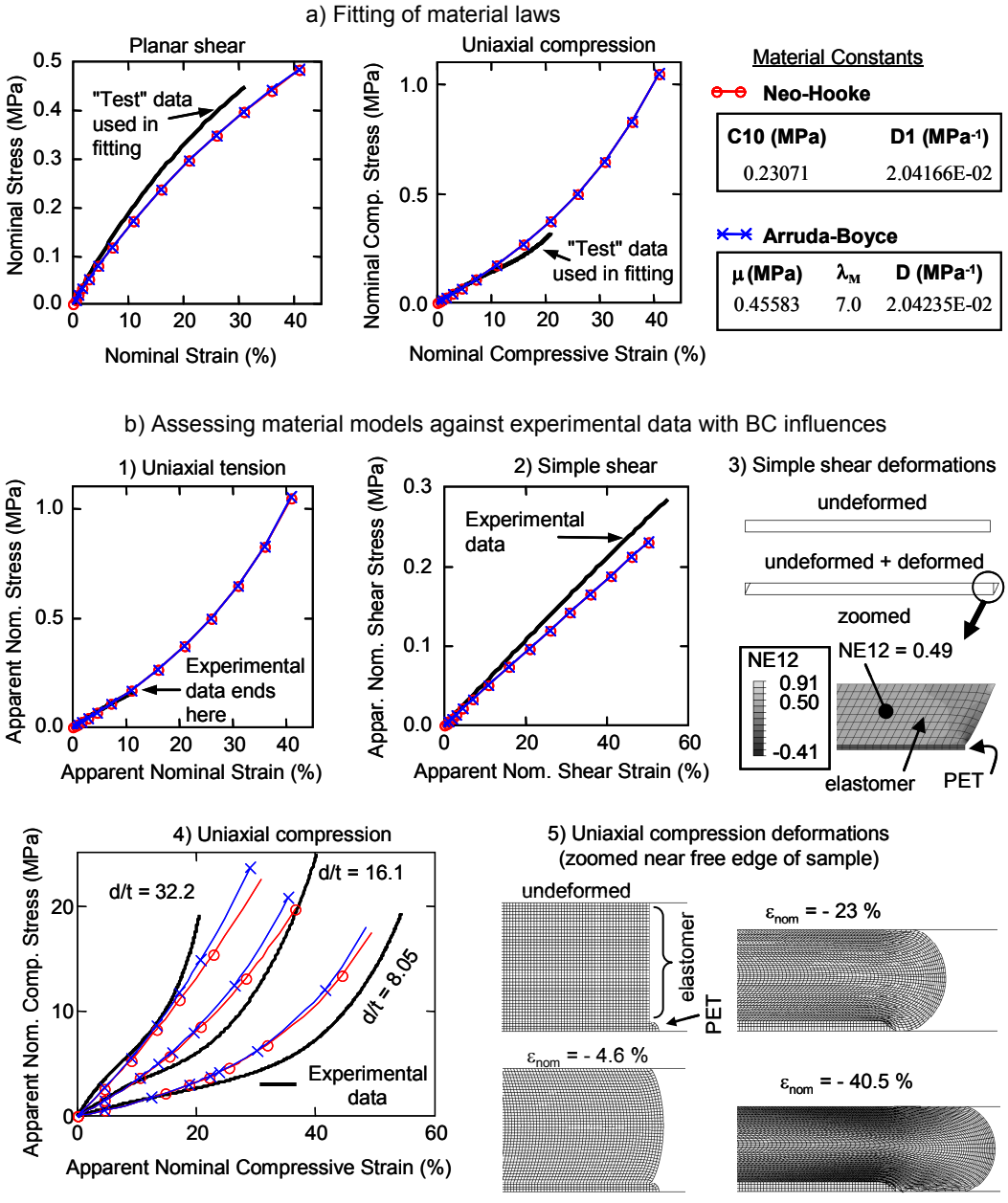

Figure 5: Results of fitting "corrected" material data and then assessing the validity of the resulting material models by simulating the original tests including the influence of the test's boundary conditions.

Figure 5b assesses the appropriateness of the material models by assessing FE models simulating the original test set-ups, including any non-ideal geometry and boundary conditions. These analyses are compared to the original test data from Figure 2, without any adjustments or corrections. While the fits are not perfect, they are considered reasonable. It is further noted that these fits are believed to be the best that are possible with this data using these material law forms.

3. Nearly incompressible elastomers reinforced by short fibers

The second material analyzed in this study is an elastomer reinforced by short fibers. The fibers are roughly oriented along the calendaring direction of the material during manufacture. The reinforced elastomer is nearly incompressible, but being fiber-reinforced, the material exhibits strong anisotropy. The desired material representation should be able to reflect both near-incompressibility and anisotropy. Specimen samples provided for testing were cubes (25.4 mm edge lengths) that were all pre-cycled to "break-in" the material. Because of constraints on specimen size and deformation modes of interest (compression and shear), both block compression and simple shear tests were performed. As before, planar (pure shear) testing was impractical due to the geometry of the supplied specimens.

Initial compression experiments were run using lubricated platens with the hope of obtaining nearly ideal test data. However, physical observations of the specimens along with Aramis non-contact surface strain measurements (www.GOM.com) demonstrated that noticeable and significant non-uniform bulging was occurring in the specimens. Additional tests estimated the coefficient of friction (COF) for the lubricated interface to range between 0.05 and 0.12 over the compression stress levels of interest. These lubricated values are much smaller than values found for dry friction which were near 1.0.

Figure 6 presents results of a FE study using 1x1x1 blocks with Neo-Hooke material models to analyze the relationship between interface friction, block bulging, actual Poisson's ratio, and *apparent* Poisson's ratio. Because transverse bulging is a non-uniform deformation, an apparent Poisson's ratio is derived from the FE results using the deformation between two face-center points as indicated in the figure. From this analysis we observe:

- For the ideal case of no friction, apparent Poisson's ratios are exactly the same as actual Poisson's ratios (as expected).
- For cases in which the COF is larger than 0.5, apparent Poisson's ratios are not dependent on COF and are the same as a no-slip condition.
- For cases in which COF is between 0 and 0.5, apparent Poisson's ratios depend on both the actual Poisson's ratio and COF.

Based on this study, it was decided that having well established boundary conditions (no slip, COF > 0.5) was more desirable than lubricated boundary conditions which induce a larger sensitivity of apparent Poisson's ratio as a function of the actual COF value. Noting that we found COF of the elastomer/metal platen interface to be near 1.0, we further established (and confirmed with physical testing) that a dry friction interface would produce the same apparent stress/strain and apparent Poisson's ratio results as a glued interface, within measurement errors and specimen repeatability. Therefore, metal/elastomer interfaces were used in all subsequent compression tests.

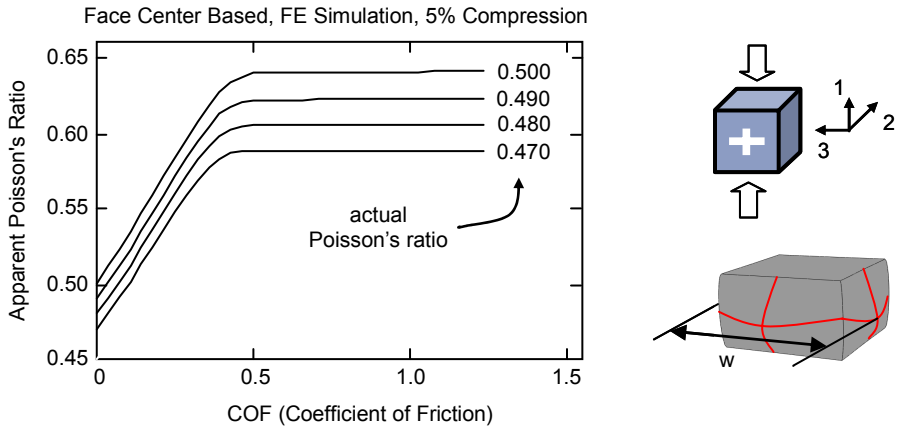

Figure 6: Finite element study of the dependence of the apparent Poisson's ratios on coefficients of friction when compressing an isotropic elastic cube (1x1x1 dimensions).

It is worth mentioning that all results shown in Figure 6 are based on simulations of compressing a cubic block. For non-cubic blocks, apparent Poisson's ratios would further depend on the block's dimension ratios.

Figure 7 depicts a small sampling of the compression and simple shear data obtained from physical testing of the short-fiber reinforced elastomer. Primary fiber reinforcement is 1-dir. Additional data not presented in the figure included sample replicates as well as other loading directions to fully quantify all the directions since the material is anisotropic. For the intended applications of this material, the maximum compressive stress was 0.345 MPa. Looking at the data, we are fortunate to observe that the material exhibits a fairly linear response within this range and that the maximum strains associated to that stress level are less than 5%. After examining the constitutive models available in Abaqus, two material models were identified for further consideration: 1) anisotropic hyperelasticity and 2) linear orthotropic elasticity.

Additional examination showed that the Holzapfel-Gasser-Odgen (HGO) anisotropic hyperelastic model, originally developed for biological tissue, was not capable of representing our reinforced elastomer. The short reinforcing fibers in our actual elastomeric material added significant stiffness when the block was compressed for small strains in the primary direction of fiber reinforcement (1-dir in Figure 7c), but then showed softening (due to fiber buckling) at larger strains. Compressing the block in the non-fiber-reinforced directions (Figure 7a-b) showed stiffer response (relative to unreinforced elastomer) due to the Poisson effect of the elastomer causing the reinforcements (predominantly in the 1-dir) to be in a tensile mode. While the HGO model can capture this latter behavior, it is not able to represent the former behavior of compression loading in the reinforcement direction because additional stiffness only occurs in the tensile modes of the reinforcement direction with the HGO model.

For the loading range of interest, short-fiber buckling is not of concern and the material data looks to be reasonably linear, although anisotropic. Using the linear orthotropic elastic model, we need

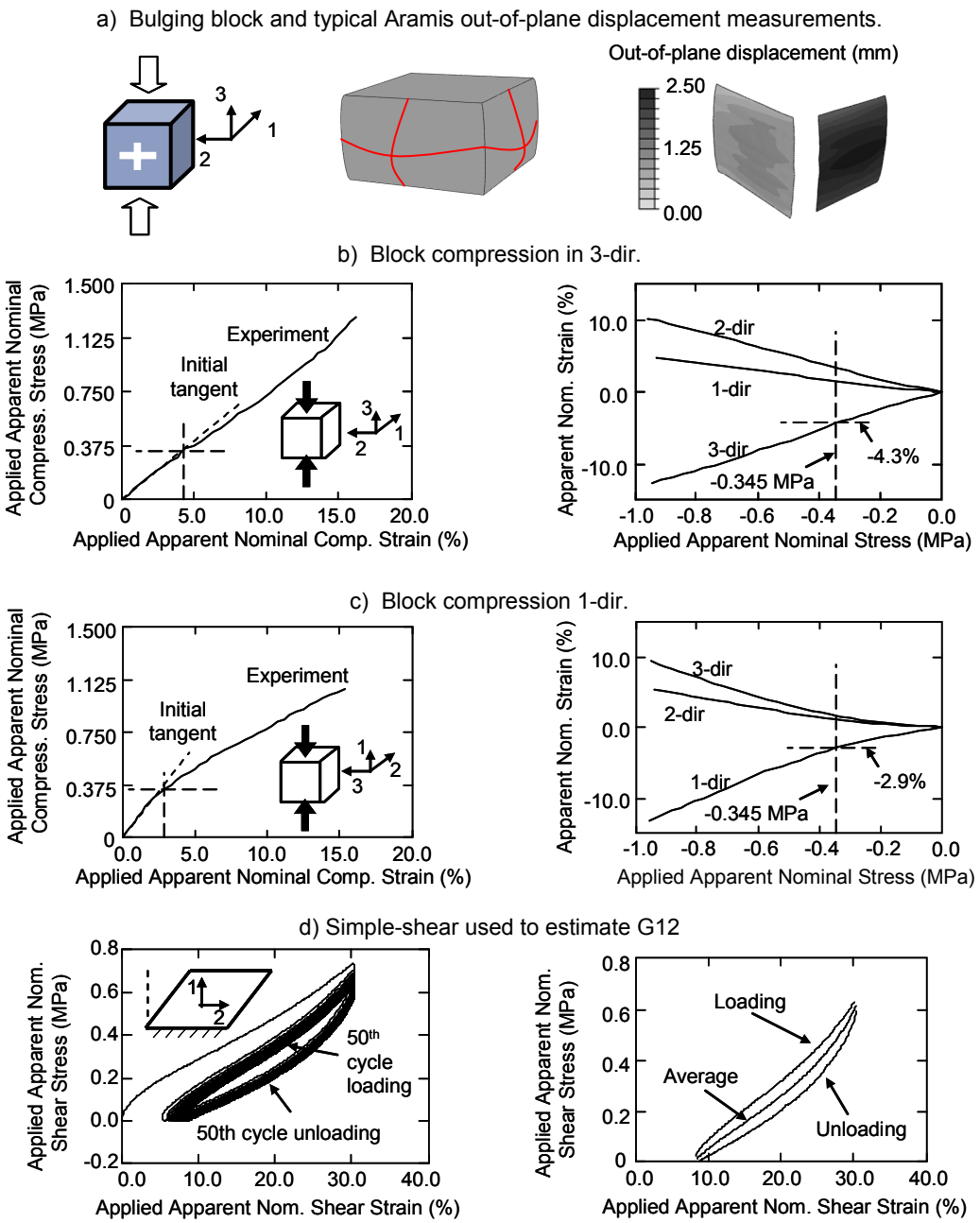

Figure 7: A representative sampling of raw test data used to characterize reinforced elastomer. All samples were cubes of length 25.4 mm. Primary fiber reinforcement is 1-dir.

data sufficient to characterize three Young's moduli, six Poisson's ratios (three of which are independent) and three shear moduli. Looking at the deformation images in Figure 7a, we see that the block compression is non-ideal due to boundary conditions inducing non-uniform bulging. As in our first case study of this paper, that means that measured stress/strain quantities are *apparent* and that adjustments or corrections will be needed.

In addition to measuring apparent applied stresses and strains, measurements of apparent transverse strains are needed to estimate the six apparent Poisson's ratio values needed for an orthotropic material. In the FE study of Figure 6 we used the face-center deformations on the deformed FE cube to obtain apparent transverse strain values. With the actual physical elastomeric blocks containing short-fiber reinforcements, it was felt that this "face-center point" measurement would introduce significant noise due to local material variations. Instead, an "average surface motion" measurement method based on Aramis surface scans was pursued. During a compression test, numerous pictures are taken of the block. These pictures are then analyzed by the Aramis system to create a discrete mesh of displacement values for the surface of the block (much like an FEA simulation). To compute average surface motion for a specific applied apparent strain, a projection algorithm was implemented to map the non-uniform bulging surfaces into uniform transverse deformations that represent the same deformed volume. Compared to the simple "face-center point" measure, this "average surface motion" measure was found to be more repeatable and less subject to local variations in the reinforced material. Using the newly developed algorithm, a gigantic amount data needed to be processed. For a typical compression test of a single specimen, 90 images are taken during the deformation (45 images per side, only two adjacent sides are measured and symmetry is assumed for their opposite sides). After image processing by Aramis, each image yields a file of 3000 to 4000 data points. Cubes must be compressed in three different directions and numerous replicates are measured to obtain a reasonable average representation of a given material type. In the complete study we ultimately assessed 13 different "reinforcement styles" (only 1 style is presented in this paper) which resulted in the processing of over 10,000 files! All of this data was analyzed and converted to apparent transverse strain values (like those in the plots of Figure 7b-c) by semi-automated Kornucopia® worksheets running in Mathcad.

Also shown in Figure 7d are the raw data from simple shear tests. As seen, the data shows hysteresis and some permanent set. Introducing complex material models to accurately capture the hysteresis response was deemed out of scope for our project, so instead an averaged apparent nominal stress-strain curve was computed by simply averaging the loading portion and unloading portion of the last cycle. From this data an initial shear modulus was estimated for each of the shear directions tested (G12, G13, G23).

From data shown in Figure 7 plus the data from the other orientations not shown, a set of apparent material constants were computed. These constants, displayed in Table 1, are *apparent* values because they are distorted from actual material constants by non-ideal boundary conditions (BCs). In addition to the distortions in the block compression data, the simple shear data has distortions also because the blocks have no applied shear stresses on the "left" and "right" sides. Simple shear loading theoretically requires shear tractions are on these surfaces too. Since the specimen dimensions are 1x1x1, the specimen geometry is likely to lead to distorted simple shear measurements (Diehl, 1995, Chapter 2.1.1). An aspect ratio of at least 10:1 (length to height) is suggested for this distortion to be considered negligible, which is clearly not the case here.

Table 1: Apparent values of material constants from data in Figure 7

Material constant	Apparent values
E_1, E_2, E_3 (MPa)	13.25, 8.260, 8.025
ν_{12}, ν_{23}, ν_{13}	0.355, 0.633, 0.529
ν_{21}, ν_{32}, ν_{31}	0.279, 0.713, 0.316
G_{12}, G_{23}, G_{13} (MPa)	2.042, 1.478, 1.542

Table 2: Target values of constants by adjusting apparent values of Table 1

Material constant	Adjusted apparent values
E_1, E_2, E_3 (MPa)	13.25, 8.260, 8.025
ν_{12}, ν_{23}, ν_{13}	0.381, 0.682, 0.527
ν_{21}, ν_{32}, ν_{31}	0.238, 0.663, 0.319
G_{12}, G_{23}, G_{13} (MPa)	2.042, 1.478, 1.542

Table 3: Estimates of actual material constants, adjusted apparent values of material constants from FEA, and relative error of adjusted apparent values from FEA to target values in iterations while finding actual material constants

n	Material constant types	Estimates of actual material constants	Adjusted apparent values of material constants from FEA	Relative error of adjusted apparent values from FEA to target values from experiments
1	E_1, E_2, E_3 (MPa)	13.25, 8.260, 8.025	14.91, 9.853, 9.687	12.6%, 19.3%, 20.7%
	ν_{12}, ν_{23}, ν_{13}	0.381, 0.682, 0.527	0.401, 0.686, 0.545	5.2%, 0.6%, 3.3%
	ν_{21}, ν_{32}, ν_{31}	0.238, 0.663, 0.319	0.265, 0.674, 0.354	11.5%, 1.8%, 10.8%
	G_{12}, G_{23}, G_{13} (MPa)	2.042, 1.478, 1.542	1.659, 1.251, 1.342	-18.8%, -15.4%, -13.0%
2	E_1, E_2, E_3 (MPa)	11.76, 6.925, 6.649	13.24, 8.432, 8.150	-0.1%, 2.1%, 1.5%
	ν_{12}, ν_{23}, ν_{13}	0.362, 0.678, 0.510	0.370, 0.663, 0.515	-2.9%, -2.8%, -2.4%
	ν_{21}, ν_{32}, ν_{31}	0.213, 0.651, 0.288	0.236, 0.640, 0.317	-0.8%, -3.3%, -0.8%
	G_{12}, G_{23}, G_{13} (MPa)	2.514, 1.746, 1.772	1.951, 1.429, 1.509	-4.5%, -3.3%, -2.1%
3	E_1, E_2, E_3 (MPa)	11.77, 6.783, 6.548	13.43, 8.418, 8.170	1.4%, 1.9%, 1.8%
	ν_{12}, ν_{23}, ν_{13}	0.373, 0.698, 0.522	0.385, 0.689, 0.536	1.2%, 1.1%, 1.6%
	ν_{21}, ν_{32}, ν_{31}	0.215, 0.674, 0.291	0.242, 0.669, 0.326	1.7%, 0.9%, 2.0%
	G_{12}, G_{23}, G_{13} (MPa)	2.632, 1.804, 1.811	2.036, 1.473, 1.542	-0.3%, -0.3%, 0.0%

Inspection of the apparent material constants in Table 1 shows that they do not satisfy reciprocal relations required for linear orthotropic elastic materials (Jones, 1975), namely

$$\frac{\nu_{12}}{E_1} = \frac{\nu_{21}}{E_2}, \qquad \frac{\nu_{13}}{E_1} = \frac{\nu_{31}}{E_3}, \qquad \frac{\nu_{23}}{E_2} = \frac{\nu_{32}}{E_3}. \tag{4}$$

Below is a measure for determining how well the reciprocal relations are satisfied:

$$\text{reciprocolCheck}(\nu, \text{E}) = \begin{bmatrix} \dfrac{\nu_{12}/E_1}{\nu_{21}/E_2} & \dfrac{\nu_{23}/E_2}{\nu_{32}/E_3} & \dfrac{\nu_{13}/E_1}{\nu_{31}/E_3} \end{bmatrix} \tag{5}$$

Values of 1 returned by the above check mean that the reciprocal relations are fully satisfied. The reciprocity check of the apparent values from Table 1 returns values of (0.794, 0.863, 1.014). Potential causes for these apparent values to fail the reciprocity check above are distortions caused non-ideal BCs (discussed earlier) and that the material is not truly orthotropic, but rather generally anisotropic. To proceed, it was assumed that material anisotropy was the dominant cause of this check being failed (results at the end of the paper will confirm the validity of this assumption).

Keeping within the pragmatic scope of the intended effort, the next issue to address is how to best adjust the apparent values to fit within a linear orthotropic framework. The approach developed was to adjust the apparent material constants so that they satisfy reciprocal relations with minimum and "equal" adjustments of the apparent Poisson's ratios. The rationale of the scheme is described as follows.

- Apparent Young's moduli and adjusted apparent Poisson's ratios should satisfy

$$\frac{\nu_{adj_{12}}}{\nu_{adj_{21}}} = \frac{E_{app_1}}{E_{app_2}}. \tag{6}$$

- The difference between an adjusted apparent Poisson's ratios and apparent Poisson's ratios should be minimized. The difference is measured by

$$Err = (\nu_{adj_{12}} - \nu_{app_{12}})^2 + (\nu_{adj_{21}} - \nu_{app_{21}})^2 \tag{7}$$

Minimizing the difference implies

$$\frac{dErr}{d\nu_{adj_{21}}} = 0 \quad \Rightarrow \quad \nu_{adj_{21}} = \frac{\nu_{app_{21}} E_{app_2}^2 + \nu_{app_{12}} E_{app_1} E_{app_2}}{E_{app_1}^2 + E_{app_2}^2} \tag{8}$$

Using this scheme apparent Poisson's ratios in Table 1 were adjusted and listed in Table 2.

The adjusted apparent values listed in Table 2 are still distorted from the *actual* material constants by non-ideal BCs. These adjusted apparent values now form the *target apparent values* that will be used in helping find *actual* material constants that best fit an orthotropic representation to the material response. Next we describe an approach to find best estimates of these material constants (removing the non-ideal BC influences).

Below is a simple iterative procedure developed in our study to back-out *actual* material constants from the measured test data.

1. Use adjusted apparent values from Table 2 as the initial estimates of actual material constants (Table 3, iteration 1): 3 E (E_1, E_2, E_3), 3 ν (ν_{12}, ν_{23}, ν_{13}), 3G (G_{12}, G_{23}, G_{13})
2. Run FE simulations of compression tests in each of the 3 directions and three simple shear tests (for G12, G13, G23). Models include actual geometries and effects of non-ideal BCs.
3. Post-process the FE results in the same way as experiments to obtain apparent values of E's, ν's, and G's. Compute adjusted apparent Poisson's ratios ν_{adj} according to Equation (8).
4. Compare 3 apparent E, 3 apparent G, and 6 adjusted apparent ν_{adj} obtained from step 3 with target apparent values from experiments (Table 2).
    a. Convergence is assumed if they match the target apparent values within a tolerance.
    b. Otherwise, use equation (9) below for the next estimate of actual material constants and then go to step 2.

$$\mathrm{ESTIMATEact}_{n+1} = \mathrm{ESTIMATEact}_{n} \times \frac{\mathrm{TARGETapp}}{\mathrm{FEAapp}_{n}} \tag{9}$$

where: n is iteration number, $\mathrm{ESTIMATEact}_n$ are estimates of actual material constants in the nth iteration, $\mathrm{ESTIMATEact}_{n+1}$ are estimates of actual material constants in the (n+1) iteration, FEAapp_n are adjusted apparent values of material constants from the nth iteration of FEA simulations, and TARGETapp are target apparent values given in Table 2.

Table 3 shows the results of using this procedure. The third column lists estimates of actual material constants for each iteration. As demonstrated, a converged set of constants is derived in three iterations through the procedure. "Converged" means that the adjusted apparent values from the FEA model converged to the adjusted apparent values from the experiment (Table 2).

For brevity, the apparent values from the FEA models (before adjustment) were not listed in Table 3 because the difference between the unadjusted apparent values (not shown) and the adjusted apparent values (shown) was small. The reciprocity check from Equation (5) applied to the FEA unadjusted apparent values returned (0.962 1.010, 0.991), (0.946 1.004, 0.982) and (0.943 1.005, 0.983) for the three iterations, respectively. Since these values are all close to unity, this implies that inherent material anisotropy was the dominant cause of the original data in Table 1 failing the orthotropic reciprocity checks and that the distortions from non-ideal BCs had only a small influence in failing orthotropic reciprocity.

4. Conclusions

This paper has presented advanced analyses for some very difficult, yet practical problems in FEA material characterization of nearly incompressible elastomers. Some of the key findings include:

- A set of equations was derived that allows the transformation of simple shear data to planar data (so-called pure shear). This was done so that Abaqus' build-in material calibration features can be used when simple shear tests are performed for hyperelastic models.

- A study based on small-strain FEA analyses of puck compression with different aspect ratios and Poisson values was utilized to efficiently adjust test data that exhibited large distortions

due to non-ideal boundary constraints. This adjustment worked well up to nearly 20% apparent nominal strain. This method was also shown to provide an alternative approach of estimating Poisson's ratio when specimens using multiple aspect ratios are analyzed.

- Performing uniaxial compression tests with a high friction value (or complete bonding) between the specimen and the loading platens produces well defined boundary conditions that can be readily compensated for during material calibration via FEA models. Conversely, using lubricated boundaries produces less reliable results as the apparent Poisson's ratio becomes highly sensitive to both the actual Poisson's ratio and the COF at the interface.
- An analytical formula was derived for use in adjusting, in a least squares manner, the Poisson ratio values for orthotropic material measurements when such data does not initially satisfy the reciprocity relationships of orthotropic elasticity.
- A simple iterative algorithm was presented that enables efficient calibration of material parameters by using FEA models to account for non-ideal BC in test data.

Our work has concentrated on the careful inspection of experimental test data and how such data can be appropriately adjusted to account for non-ideal distortions. These adjustments required integration of theoretical analyses, experimental data, and FEA simulations. To encourage full exploration of various potential routes, an appropriate set of software tools was essential. First, there was a large amount of data from many sources and in many formats that was analyzed. The data was plotted, trimmed, scaled, averaged, interpolated, extrapolated, curve-fitted, transformed, etc. In addition, equations (linear, nonlinear, and algorithms) were constantly being used and modified, or derived a new. At each step in the process, comments and findings needed to be documented along with the data, plots, equations, etc. in a natural and fast way. To accomplish the task the authors utilize Kornucopia® (www.BodieTech.com) and Mathcad (www.PTC.com) in conjunction with Abaqus (CAE, solvers, and Viewer, www.simulia.com) as a tool-suite that is specifically designed for this type of advanced, yet pragmatic, engineering analysis.

5. Acknowledgements

We greatly appreciate the excellent experimental work done by Christiane Hohenwarter, James Marek, William Coulter, Jason Bostron, and David Winmill. We acknowledge funding and project support from Carl Arnold, John Locke, Constantine Tsimpris, Florencio Gopez, Nathan Love, Derya Gulsen, and Mark Lamontia. We also wish to thank Victor Genberg for initially introducing our lead author to the topic of FEA modeling of nearly incompressible elastomers over 20 years ago – that initial mentoring has gone a long way!

6. References

1. Diehl, T., *Two-Dimensional and Three-Dimensional Analysis of Nonlinear Nip Mechanics with Hyperelastic Material Formulations*, Ph.D. dissertation, University of Rochester, Rochester NY, 1995, on-line at www.BodieTech.com.
2. Jones, R. M., *Mechanics of Composite Materials*, McGraw-Hill, 1975.